

ELECTROMAGNETIC ANALYSIS OF A BRIDGE CONFIGURED WINDING CAGE INDUCTION MACHINE USING FINITE ELEMENT METHOD

Rajkumar S. Konwar¹, Karuna Kalita^{1, *}, Atanu Banerjee¹, and Wee K. S. Khoo²

¹Mechanical Engineering Department, Indian Institute of Technology Guwahati, Guwahati 781039, India

²Electric Motor Design Ltd., 22-24 Harborough Road, Kingsthorpe, Northampton NN2 7AZ, United Kingdom

Abstract—A 2D finite element electromagnetic model that permits the simulation of a cage induction machine, involving the effects of eddy currents and coupling the field equation with the stator field-circuit equation, has been presented in this paper. Transformation matrix has been derived to incorporate specialized stator winding scheme called the bridge configured winding (BCW) in the coupled field circuit equation. The bridge configured winding scheme is capable of producing controllable transverse force by deliberately imparting asymmetric flux distribution in the machine air-gap. Steady state stator currents have been calculated using the time-stepping scheme with the rotor motion at constant speed allowing the FE model to take into account the harmonics due to the eccentricity (static) of the rotor. This work has furnished us with the 2D magnetic flux distribution in the whole finite element domain as well as sets out an electromagnetic model to study the electromechanical interaction between the eccentric rotor motion and the electromagnetic field. The results, in terms of variation of terminal currents (phase and bridge) and unbalanced magnetic pull (UMP) due to rotor eccentricity as well as asymmetric field (deliberately imparted by exciting the bridge), obtained from the simulation have been compared with analytical formulations as well as already published experimental results.

Received 22 November 2012, Accepted 23 January 2013, Scheduled 31 January 2013

* Corresponding author: Karuna Kalita (karuna.kalita@iitg.ernet.in).

1. INTRODUCTION

With progressive enhancement in the capability of computers, finite element method (FEM) has been extensively used as a research tool to analyze the electromagnetic field distribution in induction machines. Detail algebraic representations of the basic procedures involved in 2D electromagnetic field analysis have been presented by Salon et al. [1], in general for electromagnetic devices, such as, printer actuator, axisymmetric plunger, induction motor and later by Savov et al. [2] for cage induction motor. The stator end windings and the end-regions of the rotor cage are modeled by means of resistance and inductances, which are obtained from empirical formulae and from the 3D electromagnetic analysis in the end regions of the motor. Finite element method has been used for space discretization and the step-by-step or Crank-Nicolson method has been used for time discretization. The final discretized equation of the coupled field circuit equation is a system of nonlinear equation and solved at each step by the Newton-Raphson method. Similar methods have been proposed by Wang and Xie [3] and Ho et al. [4]. In this paper, the coupled field-circuit equations form the basis for electromagnetic finite element analysis. A finite-element variable time-stepping algorithm for solving the electromagnetic diffusion equation has been proposed by Ovando-Martínez et al. [5].

In the present, analysis coupled-field circuit equations have been developed for a particular three-phase induction machine equipped with a specialized stator winding scheme known as bridge configured winding which has parallel paths integrated into its winding structure in the sense that each of the phases is split into a “Wheatstone-bridge” arrangement. Currents passing diametrically through a phase in the *vertical* direction account for the main torque-producing components of stator field. Currents passing diametrically through the phase in the *horizontal* direction account for transverse forces. The parallel paths can be switched to open-circuit or closed-circuit without affecting the torque-producing function of the machine and all of the stator conductors contribute to torque-production. This particular winding scheme has been called bridge configured winding scheme (BCW) [6]. The bridge configured winding scheme has been implemented in empowering electrical rotating machines with the capacity to produce controllable transverse force in addition to their normal torque producing capacity. Usually two discrete sets of stator windings are deployed in the motor allowing the use of a standard supply to generate torque and the transverse force as described by Salazar and Stephen [7], Chiba et al. [8,9], and Laiho et al. [10].

The primary set carries the motor currents while the secondary or supplementary set carries levitation currents. Normally the supplementary winding is distributed to the stator slots in the wedge area and occupies about 10% of the total cross-sectional area of a single slot, which otherwise would have been occupied by the primary windings. However, in case of BCW a single set of winding is used to produce torque as well as transverse force. The details of bridge configured windings are given by Khoo [6].

The basic principle behind the specialized winding schemes is that a relatively small asymmetry of magnetic flux distribution, in the air gap of electrical rotating machines, creates a large net transverse force. This asymmetry may arise due to various reasons, such as, non-symmetrical stator windings, saturation phenomena, eccentric rotor, etc.. As a consequence, the rotor tends to get attracted towards the stator in the direction of the highest magnetic flux or shortest air-gap. This phenomenon is called unbalanced magnetic pull (UMP) [11]. Induction machines, which usually have very small air gaps, are especially vulnerable to slight variations in the dimensions of the stator and rotor. In other words, the magnetic field within electrical machines causes an interaction between the electrical and the mechanical dynamics of the system.

In the specialized winding schemes, the asymmetry of the flux distribution is deliberately imparted in the machine so that an additional field exists which is of a pole-pair difference with respect to the torque-producing component of the main field [12]. For instance, if p is the number of fundamental pole pairs, then the additional field should create a $(p \pm 1)$ pole pair to produce a net transverse force.

This paper presents a 2D FE model developed in MATLABTM environment that can simulate a 4-pole 3-phase cage induction machine with BCW (Figures 2 and 3). The developed model is capable to calculate unbalanced magnetic pull due to rotor eccentricity (static) as well as asymmetric field imparted by exciting the bridge. The simulation is performed by time stepping scheme with the rotor motion at constant speed involving eddy current and rotor eccentricity (parallel-static). A similar approach for a conventional cage induction machine is carried out by Pham et al. [13] and the simulated results with the experimental data were compared. Linear and isotropic magnetic material is considered. To make this linear assumption well founded, a comparatively small value of supply voltage is applied.

This paper has been divided into seven sections. Section 1 introduces the work that has been presented. Section 2 summarizes the discretized (in space) and coupled field circuit equations for a cage induction machine that forms the basis of 2D electromagnetic field

analysis. In Section 3, a specialized transformation is presented that connects the coupled field circuit equations with the bridge configured winding scheme. Time discretization, movement modeling and force calculation are briefly presented in Sections 4, 5 & 6, respectively. Finally, the results obtained, in terms of variation of terminal currents (phase and bridge) and unbalanced magnetic pull (UMP) due rotor eccentricity as well as asymmetric field (deliberately imparted by exciting the bridge), are presented in Section 7.

2. COUPLING OF ELECTROMAGNETIC FIELD EQUATION WITH THE FIELD-CIRCUIT EQUATION OF THE STATOR FOR A CAGE INDUCTION MACHINE EQUIPPED WITH SPECIAL WINDING SCHEME

The coupling of electromagnetic field equation with the field-circuit equation of the stator for a cage induction machine equipped with special winding scheme is presented in the following subsections:

2.1. Electromagnetic Field Equation for a Cage Induction Machine

The Ampere's law relating magnetic field strength \vec{H} and vector current density \vec{J} for low frequency problems can be presented as,

$$\nabla \times \vec{H} = \vec{J} \quad (1)$$

In electromagnetics, the constitutive relationship between magnetic field strength \vec{H} and magnetic flux density \vec{B} can be represented as,

$$\vec{H} = \nu \vec{B} \quad (2)$$

where ν is the magnetic reluctivity (reciprocal of magnetic permeability, μ) and is a constant for linear and isotopic magnetic material.

In the 2D finite element formulation of electromagnetic field problems, magnetic vector potential \vec{A} is commonly used. In order to satisfy the non-divergence of the magnetic field, the magnetic vector potential is defined as,

$$\vec{B} = (\nabla \times \vec{A}) \quad (3)$$

Accordingly, $\nabla \cdot (\nabla \times \vec{A}) = 0$ is satisfied for any \vec{A} . However, to define the magnetic vector potential uniquely, the Coulomb gauge is usually used, given by

$$\nabla \cdot \vec{A} = 0 \quad (4)$$

Using Equations (2) and (3) in Equation (1), the magnetic diffusion equation can be obtained as

$$\nabla \times \nu (\nabla \times \vec{A}) = \vec{J} \tag{5}$$

The present work is restricted to 2D field analysis, where \vec{J} and \vec{A} are z -directed (parallel to the axial length of the machine) and independent of z , given by

$$\vec{J} = J(x, y, t) k \tag{6}$$

$$\vec{A} = A(x, y, t) k \tag{7}$$

Here, x and y are Cartesian coordinates, k is the unit vector parallel to the z -axis and t is the time. Since, vectors \vec{J} and \vec{A} have only one component, they can be treated as scalars and Equation (5) can be represented in component form (in z -direction) as,

$$\left(\frac{\partial}{\partial x} \left(\nu \frac{\partial A}{\partial x} \right) + \frac{\partial}{\partial y} \left(\nu \frac{\partial A}{\partial y} \right) \right) = -J \tag{8}$$

The expansion of current density J [in Equation (8)] in terms of quantities relevant to the external circuit depends on the type of conductors in the FE domain. In case of a cage induction machine, current density J consists of three components: one due to the applied source, another due to the induced electric field produced by time-varying magnetic field, and the third due to relative motion-induced between the stator field and the rotor. However, the component due to relative motion can be avoided by modeling the rotor mesh in a moving frame of reference while the stator (with some fraction of the air gap) in a static frame of reference. Thus, Equation (8) becomes,

$$\left(\frac{\partial}{\partial x} \left(\nu \frac{\partial A}{\partial x} \right) + \frac{\partial}{\partial y} \left(\nu \frac{\partial A}{\partial y} \right) \right) = - \left(J^s - \sigma \frac{\partial A}{\partial t} \right) \tag{9}$$

The term J^s is associated with the component of current density due to applied source in the stator winding. Generally, the conductors of the stator winding are assumed to be filamentary and skin effect in them is neglected. The current density associated with all the points of the cross-section of a given stator coil is considered constant, whereupon the condition $\sigma = 0$ is imposed.

Let us consider a coil side $+c$ of a given coil c of the stator winding as shown in Figure 1. Assuming that the number of filamentary conductors pass through coil side $+c$ is N_{+c} . Here, N_{+c} is the number of distinct, electrically isolated current paths, with each path carrying i_{+c}^s amperes of current. Mathematically, the current density J^s for this

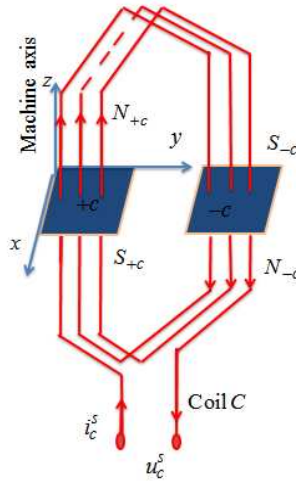


Figure 1. Representation of a coil with coil sides.

coil side $+c$ can be represented as,

$$J^s = \frac{N_{+c}}{\delta_{+c}S_{+c}}i_{+c}^s \tag{10}$$

where S_{+c} is the cross-sectional area of the coil side $+c$ and δ_{+c} ($0 < \delta < 1$) is the corresponding filling factor.

In general, for any coil side cs , the current density can be represented as

$$J^s = \frac{N_{cs}}{\delta_{cs}S_{cs}}i_{cs}^s \tag{11}$$

Introducing co-efficient $\alpha_{cs}(x, y)$, where $\alpha_{cs}(x, y) = \frac{N_{cs}}{\delta_{cs}S_{cs}}$ when the point (x, y) belongs to any coil side region (cs) and $\alpha_{cs}(x, y) = 0$ otherwise. Thus, Equation (10) becomes

$$J^s = \alpha_{cs}i_{cs}^s \tag{12}$$

Using Equation (12) in Equation (9), we get

$$\left(\frac{\partial}{\partial x} \left(\nu \frac{\partial A}{\partial x} \right) + \frac{\partial}{\partial y} \left(\nu \frac{\partial A}{\partial y} \right) \right) = - \left(\alpha_{cs}i_{cs}^s - \sigma \frac{\partial A}{\partial t} \right) \tag{13}$$

For space discretization of Equation (13), a finite element formulation of Galerkin’s method is used. For this purpose, the whole 2D cross-section (S) is discretized into a number of elements (S^e), $e = 1, 2, 3, \dots, m$ and n node.

Table 1. Elemental form of matrices $[\mathbf{S}]$, $[\mathbf{C}^r]$ and $[\mathbf{P}_{ncs}^s]$ (where k is the number of nodes in each element).

$[\mathbf{S}^e]_{k \times k} = \int_{-1}^1 \int_{-1}^1 \nu [\mathbf{B}]^T \left([\mathbf{J}]^{-T} \right) [\mathbf{J}]^{-1} [\mathbf{B}] \mathbf{J} d\xi d\eta$	This applies to all the elements in the finite element domain.
$[\mathbf{C}^{re}]_{k \times k} = \int_{-1}^1 \int_{-1}^1 \sigma \{ \mathbf{N} \} [\mathbf{N}] \mathbf{J} d\xi d\eta$ <p style="text-align: center;">ξ, λ: natural coordinates</p>	This applies to the elements only with conductivity σ (i.e., rotor bar region, r) else $[\mathbf{C}^{re}] = 0$
$[\mathbf{P}_{cs}^{se}]_{k \times 1} = \int_{-1}^1 \int_{-1}^1 \alpha_{cs} \{ \mathbf{N} \} \mathbf{J} d\xi d\eta$	This applies to the elements belonging to the thin conductor region (i.e., stator slot region) else $[\mathbf{P}_{cs}^{se}] = 0$

The method of Galerkin applied to Equation (13) yields the following global system of equations

$$[\mathbf{S}]_{n \times n} \{ \mathbf{A} \}_{n \times 1} + [\mathbf{C}^r] \frac{d}{dt} \{ \mathbf{A} \}_{n \times 1} = [\mathbf{P}_{cs}^s]_{n \times ncs} \{ \mathbf{i}_{cs}^s \}_{ncs \times 1} \quad (14)$$

where $\{ \mathbf{A} \}_{n \times 1} = [A_1 A_2 \dots A_n]^T$, $\{ \mathbf{i}_{cs}^s \}_{ncs \times 1}$ is associated with elementary coil side currents, ncs is the total number of coil sides in the stator region and the matrices $[\mathbf{S}]$, $[\mathbf{C}^r]$ and $[\mathbf{P}_{cs}^s]$ have the following elemental form as presented in Table 1.

For an k -noded element, we have

$$\{ \mathbf{A}^{ke} \} = \left\{ \begin{matrix} A_1 \\ A_2 \\ \vdots \\ A_k \end{matrix} \right\}_{k \times 1}, \text{ nodal values of } A \quad (15)$$

$$[\mathbf{N}] = [N_1 N_2 N_3 \dots N_k] = \{ \mathbf{N} \}^T, \text{ shape functions} \quad (16)$$

$$[\mathbf{J}]_{2 \times 2} = \left[\begin{matrix} \frac{\partial N_1}{\partial \xi} & \dots & \frac{\partial N_k}{\partial \xi} \\ \frac{\partial N_1}{\partial \eta} & \dots & \frac{\partial N_k}{\partial \eta} \end{matrix} \right]_{2 \times k} \left[\begin{matrix} x_1 & y_1 \\ \vdots & \vdots \\ \vdots & \vdots \\ x_k & y_k \end{matrix} \right]_{k \times 2} \quad (17)$$

$$[\mathbf{B}]_{2 \times k} = \begin{bmatrix} \frac{\partial N_1}{\partial \xi} & \cdots & \frac{\partial N_k}{\partial \xi} \\ \frac{\partial N_1}{\partial \eta} & \cdots & \frac{\partial N_k}{\partial \eta} \end{bmatrix}_{(2 \times k)} \quad (18)$$

The vector of coil side currents can be transformed in terms of terminal currents, which of course depends upon the type of stator winding used. In general, the transformation can be written as

$$\{\mathbf{i}_{cs}^s\}_{ncs \times 1} = [\mathbf{T}]_{ncs \times nter} \{\mathbf{i}_{ter}^s\}_{nter \times 1} \quad (19)$$

where, $\{\mathbf{i}_{ter}^s\}_{nter \times 1}$ is associated with the terminal currents, *ter* stands for terminal and *nter* stands for number of terminals currents. For instance, the number of terminal currents for a conventional 3-phase cage induction machine is three, i.e., *nter* = 3.

The transformation matrix $[\mathbf{T}]_{ncs \times nter}$ in Equation (19) relates the coil side currents with the terminal currents in the stator. Transformations can be obtained for different given winding schemes. Therefore, in general, the electromagnetic field equation for a cage induction machine, equipped with any given stator winding scheme, can be represented as

$$[\mathbf{S}]_{n \times n} \{\mathbf{A}\}_{n \times 1} + [\mathbf{C}^r] \frac{d}{dt} \{\mathbf{A}\}_{n \times 1} = [\mathbf{P}_{cs}^s]_{n \times ncs} [\mathbf{T}]_{ncs \times nter} \{\mathbf{i}_{ter}^s\}_{nter \times 1} \quad (20)$$

2.2. Field-circuit Equation for the Stator

When the FE discretized electromagnetic field equation is given by Equation (20), the corresponding stator field-circuit equation can be represented as

$$\begin{aligned} & [\mathbf{Q}^s]_{nter \times n} \frac{d\{\mathbf{A}\}_{n \times 1}}{dt} + [\mathbf{R}^s] \{\mathbf{i}_{ter}^s\}_{nter \times 1} + [\mathbf{L}_{end}^s] \frac{d}{dt} \{\mathbf{i}_{ter}^s\}_{nter \times 1} \\ & = \{\mathbf{u}_{ter}^s\}_{nter \times 1} \end{aligned} \quad (21)$$

where, $[\mathbf{Q}^s]_{nter \times n} = l([\mathbf{P}_{cs}^s]_{n \times ncs} [\mathbf{T}]_{ncs \times nter})^T$, $[\mathbf{R}^s]$ and $[\mathbf{L}_{end}^s]$ are the diagonal matrices representing total resistance and end winding inductance associated with each of the terminal currents. In the above formulation, the rotor circuit is not explicitly coupled because, for a cage induction machine, the rotor bars are not externally fed and they are connected and short-circuited [14]. However, the effects of eddy currents in the rotor bars is included in the above formulation and this is represented by the term “ $[\mathbf{C}^r] \frac{d}{dt} \{\mathbf{A}\}_{n \times 1}$ ” in Equation (20).

3. BRIDGE CONFIGURED WINDING SCHEME

The bridge configured winding (BCW), first introduced by Khoo [6], overcomes the drawback associated with dual set of stator secondary windings [8] by utilizing the main torque producing winding to suppress the UMP due to eccentricity. Thus, for the same performance the machine with the bridge configured windings will be smaller in size and weight than those with dual set of stator windings. The principal feature of the BCW is that the currents responsible for torque production are divided into two parallel paths in each phase as shown in Figure 2. However, it is mandatory that an appropriate isolation between the levitation supply and the mains must be enforced for the bridge connection to work [12]. Otherwise, both supplies will be shorted. When the bridge connection has more than one levitation supply, not only must each levitation supply be isolated from the mains, they must also be isolated from each other.

Figures 2 and 3 depict a 3-phase 4-pole induction motor having coils wound on a 36-tooth stator with double layer winding. Each phase has 12 full coils. $a_1, a_2, a_3, \dots, a_6$ and $aa_1, aa_2, aa_3, \dots, aa_6$ represent the twelve full coils of phase A. Each full coil has two coil sides. For an example $+a_1$ and $-a_1$ are two coil sides of full coil a_1 . Similarly, $+a_2, +a_3, \dots, +a_6$ and $-a_2, -a_3, \dots, -a_6$ are two coil sides of full coils a_2, a_3, \dots, a_6 respectively. ‘+’ sign means currents in that coil side is going down and ‘-’ sign means currents in that coil side is coming up. The three full coils a_1, a_2 , and a_3 together form a coil

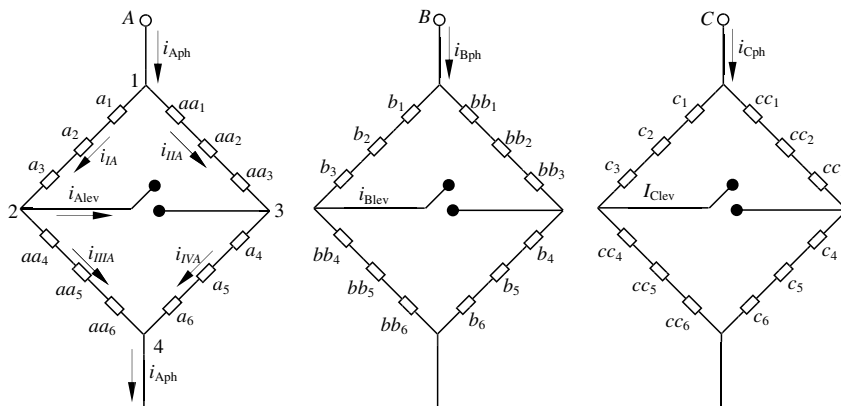


Figure 2. Stator connection of a 3-phase induction machine based on the bridge configured winding scheme [15], with simplified instantaneous current distribution in phase A.

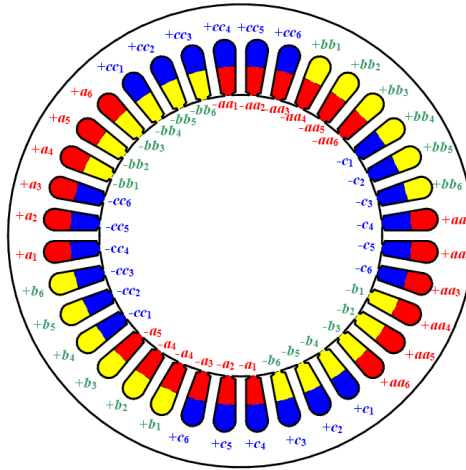


Figure 3. Stator of an induction machine with bridge configured winding. Red, blue and yellow colors show the three different phases [15].

group. Each phase has four coil groups. Coils “ $a_1, a_2, a_3, \dots, a_6$ ” are wound and aligned at the same axis of symmetry, thereby producing the same magnetic effect as having a single coil with twice the number of turns. Likewise, coils “ $aa_1, aa_2, aa_3, \dots, aa_6$ ” are wound at the diametrically opposite tooth with respect to coils “ $a_1, a_2, a_3, \dots, a_6$ ” to form a bridge and hence, the name bridge configured winding. Coils in phases “B” and “C” are connected in a similar manner and each bridge is linked to the other at one point forming an overall 3-phase star connection. The feature which makes the bridge winding different from the other active methods for reducing UMP is its provision for passive control. Passive control of UMP can be accomplished by short circuiting the additional pairs of terminals or “closing the bridge”. No current will flow across the bridge if the rotor is concentric and the stator MMF is symmetric (flux field is uniformly distributed), i.e., bridge currents are zero. Any unbalance of field due to eccentricity will induce an EMF tending to drive currents in the closed circuit such that an MMF comes to exist opposing the rate of change of this field. The currents flowing across the bridge are known as equalizing currents. Therefore, from the electrical dynamics alone we can measure the equalizing currents for an eccentric rotor. In other words, these equalizing currents are the measures of eccentricity of a particular machine at its operating conditions. More properties of the bridge configured winding can be found in Khoo [6] and Khoo et al. [12].

3.1. Coupling of Electromagnetic Field Equation with the Field-circuit Equation of the Stator for Bridge Configured Winding Cage Induction Machine

The general form of electromagnetic field equation and its corresponding stator field-circuit equation for a cage induction machine is presented in Section 2. The transformation matrix that relates the coil side currents to the terminal currents, ultimately depends upon the type of stator winding. In the present case, the stator circuit consists of 72 coil side currents and 6 terminal currents (3 terminals for phase currents and another 3 for levitation purpose). Therefore, the field Equation (20) and the stator field-circuit Equation (21) for the present bridge configured scheme (shown in Figures 2 and 3) can be represented as

$$[\mathbf{S}]_{n \times n} \{ \mathbf{A} \}_{n \times 1} + [\mathbf{C}^r] \frac{d}{dt} \{ \mathbf{A} \}_{n \times 1} = [\mathbf{P}_{cs}^s]_{n \times 72} [\mathbf{T}]_{72 \times 6} \{ \mathbf{i}_{ph+lev}^s \}_{6 \times 1} \quad (22)$$

$$[\mathbf{Q}^s]_{6 \times n} \frac{d \{ \mathbf{A} \}_{n \times 1}}{dt} + [\mathbf{R}^s] \{ \mathbf{i}_{ph+lev}^s \}_{6 \times 1} + [\mathbf{L}_{end}^s] \frac{d}{dt} \{ \mathbf{i}_{ph+lev}^s \}_{6 \times 1} = \{ \mathbf{u}_{ph+lev}^s \}_{6 \times 1} \quad (23)$$

where, $[\mathbf{Q}^s]_{6 \times n} = l([\mathbf{P}_{cs}^s]_{n \times 72} [\mathbf{T}]_{72 \times 6})^T$, $[\mathbf{R}^s]$ and $[\mathbf{L}_{end}^s]$ are the diagonal matrices representing total resistance and end winding inductance associated with each of the 6 terminal currents of the

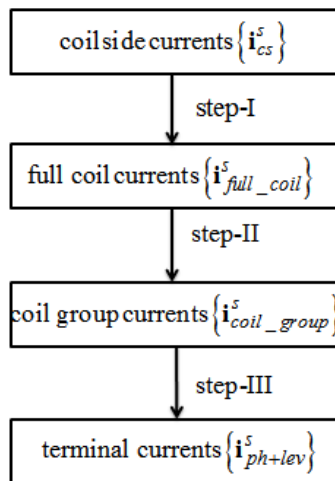


Figure 4. Transformation from coil side currents to terminal currents.

stator winding, $\{\mathbf{i}_{ph+lev}^s\} = [i_{Aph} \ i_{Alev} \ i_{Bph} \ i_{Blev} \ i_{Cph} \ i_{Clev}]^T$ and $\{\mathbf{u}_{ph+lev}^s\} = [u_{Aph} \ u_{Alev} \ u_{Bph} \ u_{Blev} \ u_{Cph} \ u_{Clev}]^T$. The transformation matrix $[\mathbf{T}]_{72 \times 6}$ in Equation (22) relates the 72 coil side currents with the 6-terminal currents. This transformation can be obtained in three steps (Figure 4) as presented in the following subsections:

3.1.1. Transformation of the Coil Side Currents to the Full-coil Currents in the Stator (Step-I)

Every full coil current corresponds to two coil side currents. In Figure 2, a_1 represents one full coil. This transformation imposes a constraint that current going down in slot $-a_1$ is equal in magnitude to the current coming up in slot $+a_1$ but opposite in sign. This transformation can be written by inspection and can be expressed as:

$$\{\mathbf{i}_{cs}^s\}_{72 \times 1} = [\mathbf{T}_{s1}]_{72 \times 36} \cdot \{\mathbf{i}_{full_coil}^s\}_{36 \times 1} \tag{24}$$

where $\{\mathbf{i}_{full_coil}^s\}$ is the vector of full coil currents. For the machine considered $\{\mathbf{i}_{full_coil}^s\}$ will have 36 entries. We can write the transformation for this as

$$\begin{Bmatrix} i_{+a_1} \\ i_{-a_1} \\ i_{+a_2} \\ i_{-a_2} \\ \vdots \end{Bmatrix} = \begin{bmatrix} 1 & 0 & \dots & \dots \\ -1 & 0 & \dots & \dots \\ 0 & 1 & \dots & \dots \\ 0 & -1 & \dots & \dots \\ \vdots & \vdots & \dots & \dots \end{bmatrix} \begin{Bmatrix} i_{a_1} \\ i_{a_2} \\ \vdots \end{Bmatrix} \tag{25}$$

where i_{+a_1} , i_{-a_1} , i_{+a_2} and i_{-a_2} are the coil side currents of coil sides $+a_1$, $-a_1$, $+a_2$ and $-a_2$ respectively and i_{a_1} , i_{a_2} are the full coil currents of full coils a_1 and a_2 respectively [refer Figures 2 and 3].

3.1.2. Transformation of the Full Coil Currents to the Coil Group Currents in the Stator (Step-II)

Let us consider the phase A (as shown in Figure 2). The three full coils a_1 , a_2 and a_3 together form one ‘‘coil group’’ and since they are connected in series, they have the same branch current i_A . Therefore, we have

$$\begin{Bmatrix} i_{a1} \\ i_{a2} \\ i_{a3} \\ i_{a4} \\ i_{a5} \\ i_{a6} \end{Bmatrix} = \begin{bmatrix} 1 & 0 \\ 1 & 0 \\ 1 & 0 \\ 0 & 1 \\ 0 & 1 \\ 0 & 1 \end{bmatrix} \begin{Bmatrix} i_A \\ i_D \end{Bmatrix}_{\text{phase A}} \tag{26}$$

Similarly we can have transformations for other coil groups. Finally the transformation that transforms the full coil currents $\{\mathbf{i}_{full_coil}^s\}_{(36 \times 1)}$ to the coil group currents $\{\mathbf{i}_{coil_group}^s\}_{(12 \times 1)}$ is:

$$\{\mathbf{i}_{full_coil}^s\}_{(36 \times 1)} = [\mathbf{T}_{s2}]_{(36 \times 12)} \{\mathbf{i}_{coil_group}^s\}_{(12 \times 1)} \quad (27)$$

3.1.3. Transformation of the Coil Group Currents to the Terminal Currents (Step-III)

Assuming the same resistance in each branch, the transformation matrix that transforms the group currents (or branch currents) to the phase currents and levitation currents for phase A is calculated as follows:

$$\left\{ \begin{array}{c} i_{IA} \\ i_{IIA} \\ i_{IIIA} \\ i_{IVA} \end{array} \right\}_{\text{phase A}} = \begin{bmatrix} 1/2 & 1/2 \\ 1/2 & -1/2 \\ 1/2 & -1/2 \\ 1/2 & 1/2 \end{bmatrix} \left\{ \begin{array}{c} i_{Aph} \\ i_{Alev} \end{array} \right\} \quad (28)$$

where i_{IA} , i_{IIA} , i_{IIIA} and i_{IVA} are the currents in four branches of the bridge for phase A.

Similar transformations shown in Equation (28) can be obtained for phases B and C. It is also assumed here that the EMFs due to changing magnetic field are identical for each branch of the bridge. Finally the transformation that transforms the coil group currents $\{\mathbf{i}_{coil_group}^s\}_{(12 \times 1)}$ to six terminal currents (two for each phase) $\{\mathbf{i}_{ph+lev}^s\}_{6 \times 1}$ is:

$$\{\mathbf{i}_{coil_group}^s\}_{(12 \times 1)} = [\mathbf{T}_{s3}]_{(12 \times 6)} \{\mathbf{i}_{ph+lev}^s\}_{6 \times 1} \quad (29)$$

Combining the three steps (Equations (24), (27) and (29)) the final expression for $\{\mathbf{i}_{cs}^s\}$ can be derived as

$$\begin{aligned} \{\mathbf{i}_{cs}^s\}_{72 \times 1} &= [\mathbf{T}_{s1}]_{72 \times 36} \cdot \{\mathbf{i}_{full_coil}^s\}_{36 \times 1} \\ &= [\mathbf{T}_{s1}]_{72 \times 36} [\mathbf{T}_{s2}]_{36 \times 12} \{\mathbf{i}_{coil_group}^s\}_{12 \times 1} \\ &= [\mathbf{T}_{s1}]_{72 \times 36} [\mathbf{T}_{s2}]_{36 \times 12} [\mathbf{T}_{s3}]_{12 \times 6} \{\mathbf{i}_{ph+lev}^s\}_{6 \times 1} \\ &= [\mathbf{T}_s]_{72 \times 6} \cdot \{\mathbf{i}_{ph+lev}^s\}_{6 \times 1} \end{aligned} \quad (30)$$

4. SOLUTION OF THE COUPLED FINITE ELEMENT EQUATIONS BY CRANK-NICOLSON TIME DISCRETIZATION METHOD

To solve the system of ordinary differential equations given by Equation (22) and Equation (23), time-discretization schemes Crank-Nicolson method is used. It is a second-order finite difference

method, implicit in time and is unconditionally stable. After applying Crank–Nicolson time discretization to Equation (22) and Equation (23), respectively. The final expression in matrix form can be written as

$$\begin{aligned} & \left[\begin{array}{cc} \left([\mathbf{S}]^{t+\Delta t} + \frac{2}{\Delta t} [\mathbf{C}^r] \right) & -[\mathbf{P}^s] \\ \frac{2}{\Delta t} [\mathbf{Q}^s] & ([\mathbf{R}^s] + \frac{2}{\Delta t} [\mathbf{L}_{\text{end}}^s]) \end{array} \right] \{\mathbf{X}\}^{t+\Delta t} \\ = & - \left[\begin{array}{cc} ([\mathbf{S}]^t - \frac{2}{\Delta t} [\mathbf{C}^r]) & -[\mathbf{P}^s] \\ -\frac{2}{\Delta t} [\mathbf{Q}^s] & ([\mathbf{R}^s] - \frac{2}{\Delta t} [\mathbf{L}_{\text{end}}^s]) \end{array} \right] \{\mathbf{X}\}^t + \{\mathbf{F}\}^{t+\Delta t} + \{\mathbf{F}\}^t \quad (31) \end{aligned}$$

where, $\{\mathbf{F}\} = \left\{ \begin{array}{l} \{\mathbf{0}\}_{n \times 1} \\ \{\mathbf{u}_{ph+lev}^s\}_{6 \times 1} \end{array} \right\}_{(n+6) \times 1}$, $\{\mathbf{X}\} = \left\{ \begin{array}{l} \{\mathbf{A}\}_{n \times 1} \\ \{\mathbf{i}_{ph+lev}^s\}_{6 \times 1} \end{array} \right\}_{(n+6) \times 1}$ and $[\mathbf{P}^s] = [\mathbf{P}_{cs}^s]_{n \times 72} [\mathbf{T}]_{72 \times 6}$. In this system of equations, there are no more time derivatives. Furthermore, all the terms on the right hand side are known either as source terms or from the field solution at the previous time step.

4.1. Boundary Condition

The magnetic vector potential A is zero on the outer boundary and inner boundary, which means that the magnetic flux density has no normal components on the boundary. The insertion of boundary condition is performed when the global matrices are fully assembled.

5. ACCOMMODATION OF MOVEMENT MODELING USING AIR-GAP STITCHING METHOD

In the present analysis, air-gap stitching method is used for modeling the rotor movement. In this method, the rotor and stator are modeled using completely separate FEA models — each including some fraction of the air gap. The two subsystem models are combined by stitching the outer diameter of the rotor and the inner diameter of the stator in the air gap. Quadrilateral quadratic finite elements are used to model the stator and rotor while second-order triangular elements have been incorporated for air-gap stitching (shown in Figure 5). During the simulation, at least some of the airgap has to be re-meshed to account for the rotor movement. This means that the element matrices for (some of) the airgap must be derived at every time step during the simulation even if the magnetic saturation is not considered. At the very least, one whole radial layer of airgap elements will have to be derived afresh. A strong advantage of this method is that it can cope with the case of eccentric rotor and stator provided that the eccentricity is smaller than the thickness of the stitched band. This

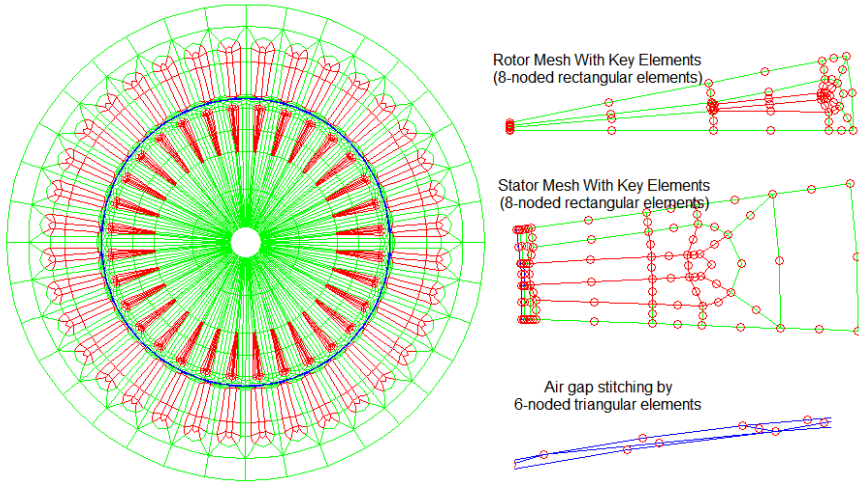


Figure 5. Finite element mesh with key-elements.

type of movement modeling has been adopted in various publications, such as Pham et al. [13] and later by Kalita [15].

6. CALCULATION OF UMP ACTING ON THE ROTOR

At first, the components of magnetic flux density \vec{B} are calculated from the magnetic vector potential \vec{A} using Equation (3), i.e., for a given element e with k nodes we get,

$$\vec{B}^e = \nabla \times \vec{A}^e = +\frac{\partial A^e}{\partial y} \hat{i} - \frac{\partial A^e}{\partial x} \hat{j} \tag{32}$$

So, the magnetic flux density along x -direction and y -direction are respectively

$$\left. \begin{aligned} B_x^e &= +\frac{\partial A^e}{\partial y} \\ B_y^e &= -\frac{\partial A^e}{\partial x} \end{aligned} \right\} \tag{33}$$

where, $\left\{ \begin{matrix} \frac{\partial A^e}{\partial x} \\ \frac{\partial A^e}{\partial y} \end{matrix} \right\} = [\mathbf{J}]^{-1} \cdot \left[\begin{matrix} \frac{\partial N_1}{\partial \xi} & \cdots & \frac{\partial N_k}{\partial \xi} \\ \frac{\partial N_1}{\partial \eta} & \cdots & \frac{\partial N_k}{\partial \eta} \end{matrix} \right] \left\{ \begin{matrix} A_1 \\ A_2 \\ \vdots \\ A_k \end{matrix} \right\}$, and $[\mathbf{J}]$ is the

Jacobian matrix given by Equation (17).

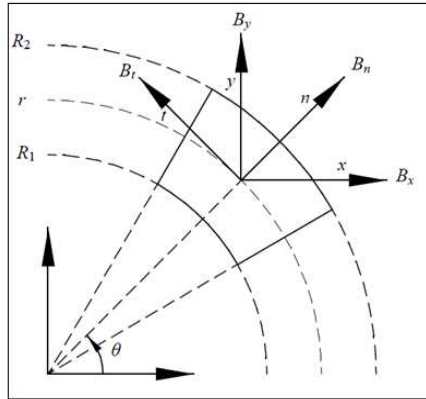


Figure 6. Components of magnetic flux density.

From the Cartesian components of \vec{B} , its normal component B_n and tangential component B_t can be obtained as follows (Figure 6):

$$\left. \begin{aligned} B_n &= B_x \cos \theta + B_y \sin \theta \\ B_t &= -B_x \sin \theta + B_y \cos \theta \end{aligned} \right\} \quad (34)$$

Using the normal and tangential components of magnetic flux density, the normal and tangential components of the Maxwell’s stress in the air gap can be obtained as

$$\left. \begin{aligned} \sigma_n &= \frac{B_n^2 - B_t^2}{2\mu_0} \\ \tau_t &= \frac{2B_n B_t}{2\mu_0} \end{aligned} \right\} \quad (35)$$

If a circle of radius r is taken as the integration path (Figure 6). The forces can be represented as (l is the axial length of the machine)

$$F_x = l \int_0^{2\pi} (\sigma_{nn} \cos \theta - \tau_{tt} \sin \theta) r d\theta \quad (36)$$

$$F_y = l \int_0^{2\pi} (\sigma_{nn} \sin \theta + \tau_{tt} \cos \theta) r d\theta \quad (37)$$

7. RESULTS OBTAINED

Taking a 3-phase squirrel cage induction machine as example (Figures 2 and 3), finite element modeling has been done with the bridge

configured winding scheme. Some important parameters of the machine under consideration are shown in Table 2.

In the present work, a 2D finite element code has been developed in MATLABTM environment that can simulate and solve the differential equations of a bridge configured squirrel-cage induction machine. The code comprises of a pre-processor where the model is built; a solver where excitations (phase and bridge voltages) are applied and responses are computed; and a postprocessor for producing graphical output.

The simulation has been performed by the time stepping scheme with the rotor motion at constant speed allowing the FE model to take into account the harmonics due to the eccentric (static) rotor motion. Besides, the simulation is performed applying 3-phase sinusoidal voltages at the stator terminals and bridge terminals (both separately and simultaneously) at different conditions of slip (2% slip and locked rotor), bridge-configuration and eccentricity of the rotor. Some important results have been observed from the FE code as presented in the following sub-sections.

Table 2. Important parameters of the machine under consideration (Kalita [15]).

Parameters	Value/Type
Number of poles	4
Number of phase	3
Number of stator slots	36
Outer diameter of the stator [mm]	152
Inner diameter of the stator [mm]	90
Number of rotor slots	32
Outer diameter of the rotor [mm]	89.2
Air gap radial thickness [mm]	0.4
Length of the rotor [mm]	123
Rotor winding	Squirrel cage un-skewed
Stator winding (6/9 pitch coil)	Bridge configured double layer
Resistance per phase [Ohm]	0.6633

7.1. Flux Distribution due to Torque-producing Field and Levitation Field

The main objective of BCW in an electrical machine is to produce controllable transverse force. For a net transverse force to be accomplished in the machine, it is mandatory that the component of levitation flux must be a pole-pair different ($p \pm 1$) to that of the torque-producing component of flux. This leads to the following conclusions (with reference to the connection shown in Figures 2 and 3):

- Excitation of the phase terminals with bridge terminals open should result in a 4-pole flux distribution as shown in Figure 7 (with concentric rotor).
- Keeping the phase terminal open and exciting the bridges should produce a combination of 2-pole $\{2 \times (p - 1)\}$ and 6-pole $\{2 \times (p + 1)\}$ flux distribution as presented in Figures 7 and 8. Here, p is the number of fundamental pole pairs, in the present case $p = 2$, i.e., four fundamental poles.

7.2. Bridge Currents or Levitation Currents

If the rotor happens to be concentric and if the stator is electromagnetically symmetric, there will be no equalizing currents even if the equalizing links are short circuited.

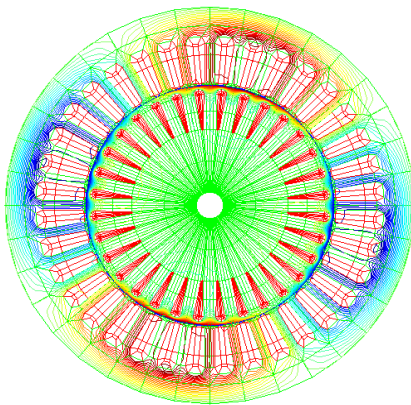


Figure 7. 4-pole flux distribution due to main field excitation only.

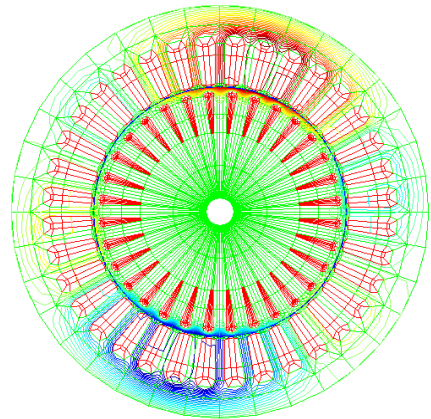


Figure 8. Combination of 2-pole $2 \times (p - 1)$ and 6-pole $2 \times (p + 1)$ flux distribution due to levitation field excitation only.

Figure 9 shows the variation of phase voltages, phase currents and levitation currents for a concentric rotor with short-circuited bridge, 2% slip, and 20 V at 25 Hz supply voltage. Under this condition, the levitation currents are found to be zero as predicted. The phase currents obtained from the FE-code are in good agreement with the experimental results presented by Kalita [15] for the same specification of the machine.

The rotor of the machine is shifted from the center by a known percentage of air-gap thickness along x -direction (or y -direction) to incorporate rotor eccentricity. However, the eccentricity obtained in this way is static and parallel.

In case of an eccentric rotor, obviously, there will be no net equalizing currents flowing when the equalizing links are not short circuited. Once the equalizing links have been short circuited, any unbalance of field (due to rotor eccentricity) present will induce an EMF tending to drive currents in the closed circuit. The dominant frequency components of the induced equalizing or levitation currents are given by Equation (38) (Nandi et al. [16])

$$f_{lev} = f_{sup} \pm f_{rot} \tag{38}$$

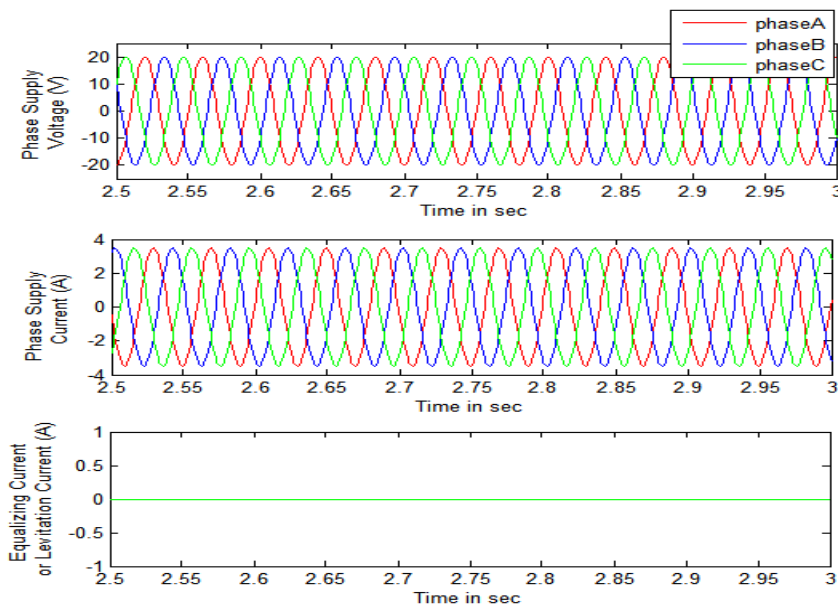


Figure 9. Variation of voltages and currents (concentric rotor, bridge short-circuited, slip 2%, and supply voltage 20 V at 25 Hz).

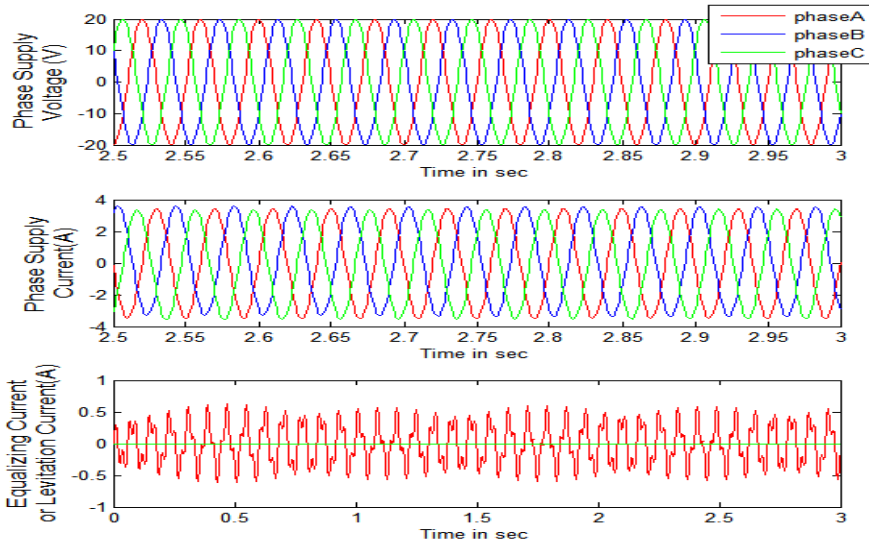


Figure 10. Variation of voltages and currents (eccentric rotor 20%, slip 0.02, supply voltage 20 V at 25 Hz, Bridge A short-circuited with other bridges left open).

where, $f_{rot} = \{(1 - s) \times \frac{f_{sup}}{p}\}$, f_{sup} = supply frequency, p = fundamental pole pair, f_{rot} = rotational frequency of the machine and s = slip.

Figure 10 shows the variation of phase voltages, phase currents and levitation current (phase A) for an eccentric (20% static) rotor with bridge A short-circuited (and other bridges left open), 2% slip, and 20 V at 25 Hz supply voltage. The corresponding frequency components of voltage and current for phase A are presented in Figure 11.

Figure 13 shows the variation of phase voltages, phase currents and levitation current (phase A) for an eccentric (20% static) rotor with Bridge A supplied with 2 V at 20 Hz (and other bridges left open), 2% slip, and 20 V at 25 Hz supply voltage. The corresponding frequency components of voltage and current for phase A are presented in Figure 14.

Figure 16 shows the variation of phase voltages, phase currents and levitation current (phase A) for an eccentric (20% static) rotor with Bridge A supplied with 2 V at 20 Hz (and other bridges left open), locked rotor, and 20 V at 25 Hz supply voltage. The corresponding frequency components of voltage and current for phase A are presented in Figure 17.

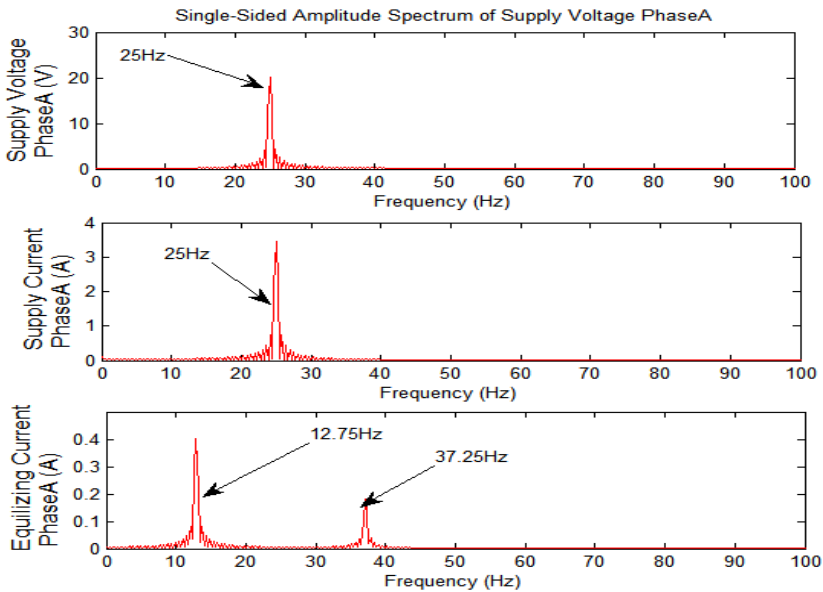


Figure 11. Single sided amplitude spectrum of voltage and current (eccentric rotor 20%, slip 0.02, supply voltage 20 V at 25 Hz, Bridge A short-circuited with other bridges left open).

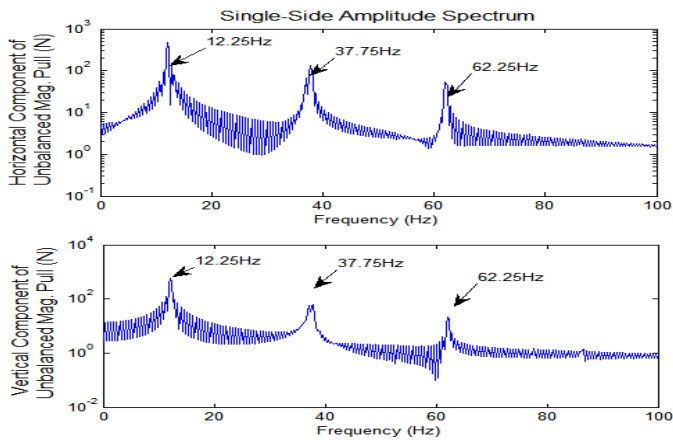


Figure 12. Components of UMP acting on the rotor (eccentric rotor 20%, slip 0.02, supply voltage 20 V at 25 Hz, Bridge A short-circuited with other bridges left open).

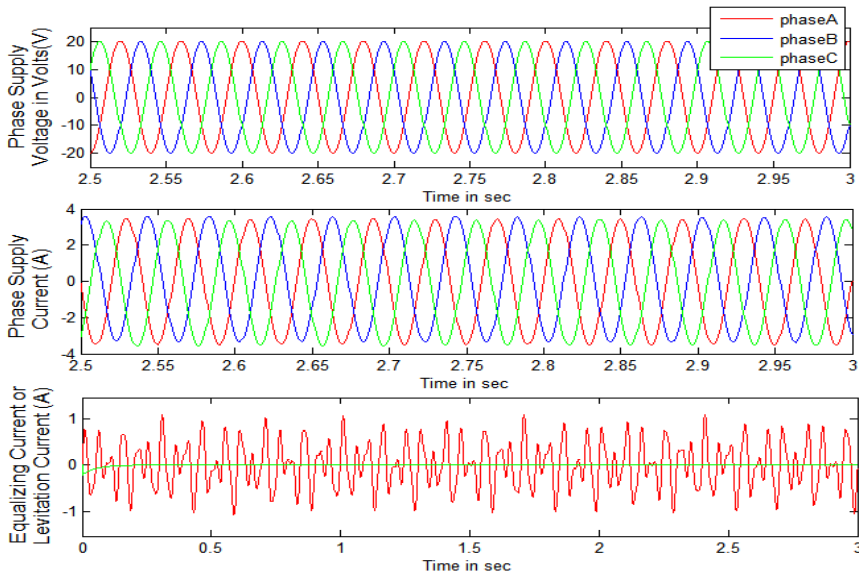


Figure 13. Variation of voltages and currents (eccentric rotor 20%, slip 0.02, supply voltage 20 V at 25 Hz, Bridge A supplied with 2 V at 20 Hz with other bridge left open).

It may be noted that the frequency components of voltage and current depicted in Figures 11, 14 and 17 are in good accordance with the analytical formulation presented in Equation (38).

7.3. Transverse Force Generated due to the Interaction between Main Field and Levitation Field

The bridge configured winding scheme has the capability to produce passive control to reduce UMP along with its provision for active control. In either of these cases, the dominant frequency components of transverse force are at $(\pm f_{sup} + f_{lev})$ generated by interaction between $\{2 \times (p - 1)\}$ pole and $(2 \times p)$ pole fields and at $(\pm f_{sup} - f_{lev})$ generated by interaction between $\{2 \times (p + 1)\}$ pole and $(2 \times p)$ pole fields [17].

Figures 12, 15, and 18 represent the frequency components of UMP obtained from the simulation of the FE-code under different operating conditions. It is observed that the frequency components of UMP obtained from the simulation are in good agreement with the analytical formulation presented by Kalita and Laiho [17].

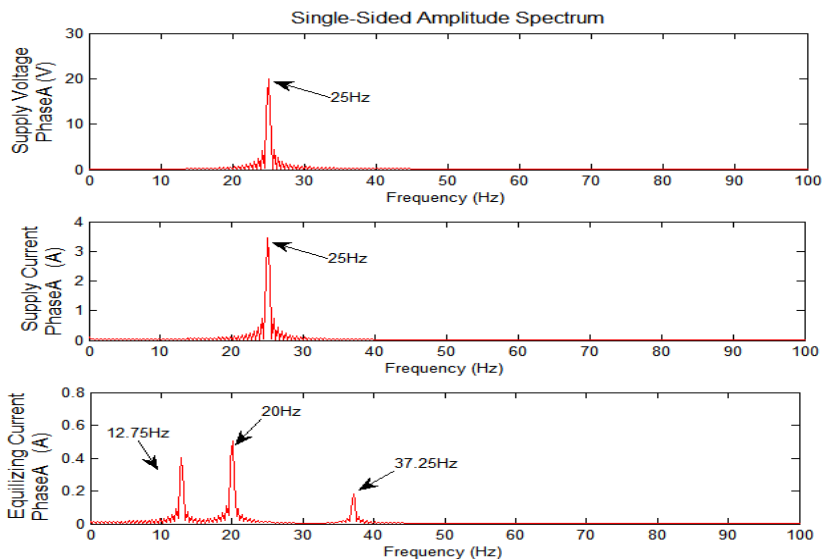


Figure 14. Single sided amplitude spectrum of voltage and current (eccentric rotor 20%, slip 0.02, supply voltage 20 V at 25 Hz, Bridge A supplied with 2 V at 20 Hz with other bridge left open).

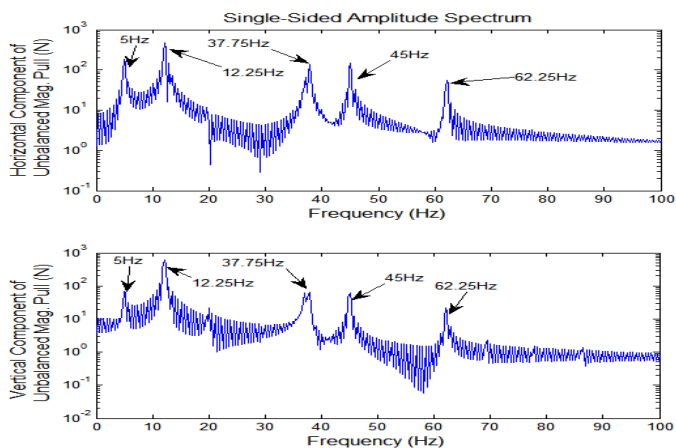


Figure 15. Components of UMP acting on the rotor (eccentric rotor 20%, slip 0.02, supply voltage 20 V at 25 Hz, Bridge A supplied with sinusoidal voltage of 2 V at 20 Hz with other bridges left open).

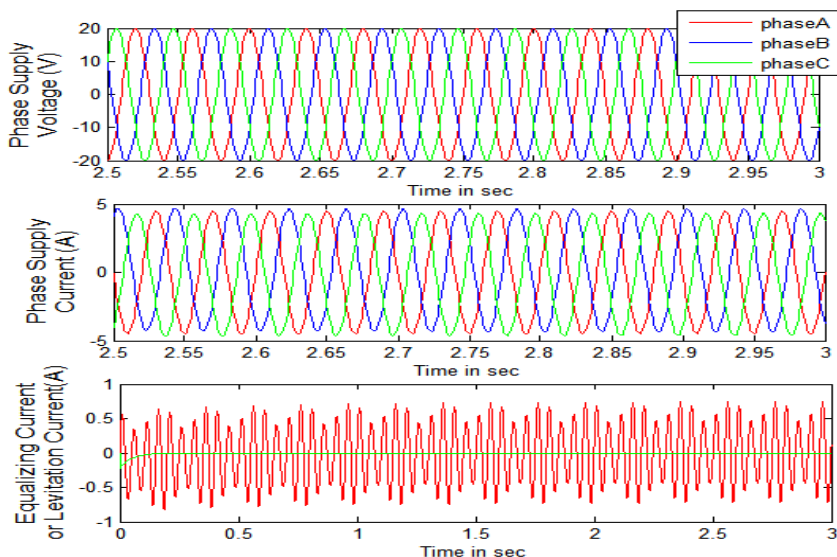


Figure 16. Variation of voltages and currents (eccentric rotor 20%, locked rotor slip = 1, supply voltage 20 V at 25 Hz, Bridge A supplied with 2 V at 20 Hz with other bridge left open).

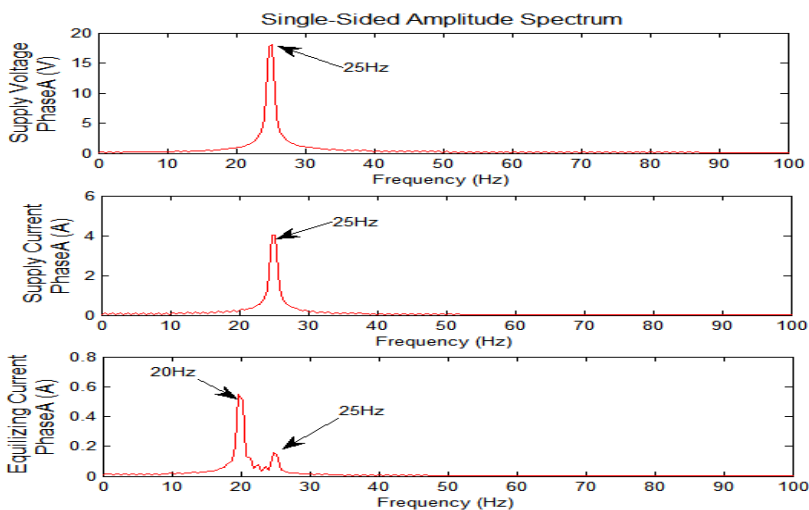


Figure 17. Single sided amplitude spectrum of voltage and current (eccentric rotor 20%, locked rotor slip = 1, supply voltage 20 V at 25 Hz, Bridge A supplied with 2 V at 20 Hz with other bridge left open).

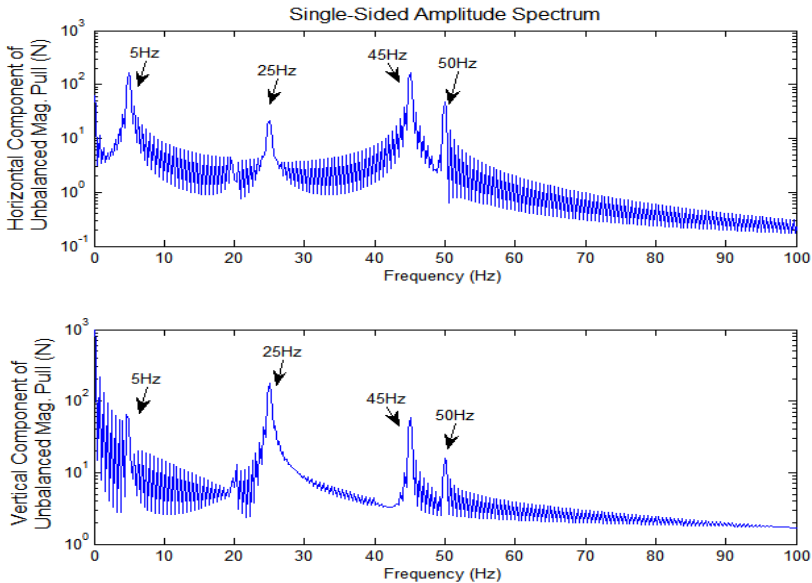


Figure 18. Components of UMP acting on the rotor (eccentric rotor 20%, locked rotor slip = 1, supply voltage 20 V at 25 Hz, Bridge A supplied with sinusoidal voltage of 2 V at 20 Hz with other bridges left open).

8. CONCLUSION

A general method for 2D finite element analysis of a cage induction machine equipped with specialized winding is presented. This method involves a transformation matrix that relates the coil side elementary currents to the terminal currents of the stator winding and can be easily derived for any given stator winding. Besides, the detail derivation of this transformation matrix with reference to a BCW is performed.

The results obtained from the FE-code developed for a BCW cage induction machine have been presented. Basically, the effect of equalizing currents (applied to the bridge) on the magnetic field coupled with rotor eccentricity (static) is shown and hence the signature of the forces developed is presented. The simulated results, in terms of variation of phase currents and frequency components of UMP due rotor eccentricity as well as asymmetric field, are found to be in good agreement when compared with analytical formulations as well as experimental results.

REFERENCES

1. Salon, S. J., M. J. DeBortoli, and R. Palma, "Coupling of transient fields, circuits, and motion using finite element analysis," *Journal of Electromagnetic Waves and Applications*, Vol. 4, No. 11, 1077–1106, 1990.
2. Savov, V. N., Z. D. Georgiev, and E. S. Bogdanov, "Analysis of cage induction motor by means of the finite element method and coupled system of field, circuit and motion equations," *Electrical Engineering*, Vol. 80, 21–28, Springer-Verlag, 1997.
3. Wang, X. and D. Xie, "Analysis of induction motor using field-circuit coupled time-periodic finite element method taking account of hysteresis," *IEEE Transactions on Magnetics*, Vol. 45, No. 3, 1740–1743, 2009.
4. Ho, S. L., S. Niu, W. N. Fu, and J. Zhu, "A power-balanced time-stepping finite element method for transient magnetic field computation," *IEEE Transactions on Magnetics*, Vol. 48, No. 2, 291–294, 2012.
5. Ovando-Martínez, R. B. B., M. A. Arjona López, and C. H. Flores, "A finite-element variable time-stepping algorithm for solving the electromagnetic diffusion equation," *IEEE Transactions on Magnetics*, Vol. 48, No. 2, 647–650, 2012.
6. Khoo, W. K. S., "Bridge configured winding for poly-phase self-bearing machines," *IEEE Transactions on Magnetics*, Vol. 41, No. 4, 1289–1295, 2005.
7. Salazar, A. O. and R. M. Stephan, "A bearing-less method for induction machine," *IEEE Transactions on Magnetics*, Vol. 29, No. 6, 2965–2967, 1993.
8. Chiba, A., T. Deido, T. Fukao, and M. A. Rahman, "An analysis of bearingless AC motors," *IEEE Transactions on Energy Conversion*, Vol. 9, No. 1, 61–67, 1994.
9. Chiba, A., K. Sotome, Y. Iiyama, and M. A. Rahman, "A novel middle-point-current-injection-type bearing-less PM synchronous motor for vibration suppression," *IEEE Transactions on Industrial Applications*, Vol. 47, No. 4, 1700–1706, 2011.
10. Laiho, A., K. Tammi, J. Orivuori, A. Sinervo, K. Zenger, and A. Arkkio, "Electromechanical interaction in eccentric-rotor cage induction machine equipped with a self-bearing force actuator," *Journal of System Design and Dynamics*, Vol. 3, No. 4, 519–529, 2009.
11. Holopainen, T., A. Tenhunen, and A. Arkkio, "Electromechanical interaction in rotor-dynamics of cage induction motors," *Journal*

- of Sound Vibration*, Vol. 284, 733–755, 2005.
12. Khoo, W. K. S., K. Kalita, and S. D. Garvey, “Practical implementation of the bridge configured winding for production of controllable transverse forces in electrical machines,” *IEEE Transactions on Magnetics*, Vol. 47, No. 6, 1712–1718, 2011.
 13. Pham, T. H., P. F. Wendling, S. J. Salon, and H. Acikgoz, “Transient finite element analysis of an induction motor with external circuit connections and electromechanical coupling,” *IEEE Transactions on Magnetics*, Vol. 14, No. 4, 1407–1412, 1999.
 14. Bastos, J. P. A. and N. Sadowski, “Electromagnetic modeling by finite element methods,” Founding Edition, 490, Marcel Dekker, Inc., New York, USA, 2003, ISBN: 0-8247-4269-9.
 15. Kalita, K., “Integrating rotor-dynamic and electromagnetic dynamic models for flexible-rotor electrical machines,” Ph.D. Thesis, The University of Nottingham, 2007.
 16. Nandi, S., R. M. Bharadwaj, and H. A. Toliyat, “Performance Analysis of a three-phase induction motor under mixed eccentricity condition,” *IEEE Transactions on Energy Conversion*, Vol. 17, No. 3, 392–399, 2002.
 17. Kalita, K. and A. Laiho, “Dynamics of bridge-configured built-in force actuator for vibration control in four-pole cage induction machine,” *National Symposium on Rotor Dynamics*, Chennai, India, December 19–21, 2011.